MONTE-CARLO EVALUATION OF CONTROL LAW FOR HIGH ALTITUDE FLIGHT TEST OF MARS AIRPLANE

Koji Fujita*, Hiroki Nagai*, Hiroshi Tokutake, and Akira Oyama*****
***Institute of Fluid Science, Tohoku University, Sendai, Miyagi, 980-8579, Japan**
****Kanazawa University, Kanazawa, Ishikawa, 920-1192, Japan**
*****Institute of Space and Astronautical Science, Japan Aerospace Exploration Agency (JAXA), Sagamihara, Kanagawa, 252-5210, Japan**

Keywords: *UAV, Monte-Carlo simulation, Flight test, Control, Flight simulation*

Abstract

A Monte-Carlo simulation is performed to evaluate the success probability of the flight test of the Mars airplane at high altitude atmosphere on Earth. The number of the uncertainty parameters is 136. The simulation result shows that the success probability is 95%. It is clarified that the most severe criterion is a maximum Mach number.

1 Introduction

Airplanes has been payed attention as a new platform for a Mars exploration [1,2]. A high altitude flight test that simulates a Martian atmospheric condition was conducted in June 2016 [3]. The high altitude flight test has various uncertainties: initial conditions such as an attitude, environmental conditions such as an atmospheric density, etc. This research evaluates a control law of the airplane using a success probability of the flight test through Monte-Carlo simulations with the various uncertainties.

2 Overview of Flight Test

The high altitude flight test was conducted at the JAXA's Taiki Aerospace Research Field in Hokkaido, Japan. Because this test was the first trial, the objective of the test was to perform basic maneuvers and to obtain the aerodynamic characteristics, especially focused on the lift coefficient. Therefore, this airplane had no propulsion system. The control surfaces of this airplane were ailerons, rudders, and an elevator. The flight test was conducted above the sea for the safety reason. First, the airplane was ascended to 36 km height by a balloon. Here, the airplane had been hanged inside the gondola to be protected from strong sunlight and cold atmosphere. After the health check, the airplane was released from the gondola and started dropping with aiming its nose downwards. Then the airplane performed the roll and pull-up maneuvers. The desired heading ψ_c was set to 127 degrees (clockwise from north), i.e. the direction from land to sea, for the safety reason. The airplane was controlled to pull-up toward this direction. After pull-up, the airplane performed a gliding flight to obtain aerodynamic characteristics at quasi-steady state. The gliding phase included three sub-phases. The airplane was glided at the trim conditions with angle of attack of 2, 4, and 6 degrees. The measurement time was around 30 seconds per each sub-phase. At two minutes after from the airplane release, the parachute was released and the airplane was slowly descended to the sea. Available sensors for the control were the 3-axial rate gyro and the dynamic pressure sensor on the airplane, and the 2-axial magnetic compasses on the airplane and the gondola. There was no communication between the gondola and the released airplane; therefore the data of the magnetic compass on the gondola was delivered just before the release and used as an initial condition.

3 Control law

The control procedure of the airplane contains three phases: a roll phase, a pull-up phase, and a glide phase.

In the roll phase, the roll motion of the airplane was controlled to aim its upper surface to the desired direction to pull-up the airplane to the desired direction. Only the ailerons were used for this maneuver. The desired roll rate P_c was obtained by the following equation:

$$P_c = A\,\mathrm{ShiftAngle}\,(\psi_c - \psi_{up}) \quad (1)$$

where

$$\psi_{up} = \psi_0 + \sum P\Delta t \quad (2)$$

here, a function "ShiftAngle(x)" converts an angle x [rad] into -π to π (e.g. ShiftAngle(1.5π) = -0.5π). A is a sensitivity coefficient. An initial heading ψ_0 was measured by the compass on the gondola. The upper surface direction was estimated by the integral of the roll rate. Usually, the integral of the output of the rate gyro is not accurate. However, the integral is acceptable for this case because the integral time is short. The nominal ailerons deflection angle in the roll phase $da_{Rollnom}$ was controlled to follow the roll rate P to the desired roll rate P_c by the following Proportional-Integral (PI) controller:

$$da_{Rollnom} = Kap_{Roll}(P_c - P) + KaIp_{Roll}\sum(P_c - P)\Delta t \quad (3)$$

here, Kap_{Roll} and $KaIp_{Roll}$ were the roll rate proportional and integral gains for the aileron in the roll phase. t is time. Note that, however, all control surfaces were fixed for the first 2 seconds to prevent from contacting with the gondola. As a longitudinal control, the elevator deflection angle was fixed to -15 degrees based on trim data of the aerodynamic model.

In the pull-up phase, both the ailerons and the rudders were used for a stabilization control. Note that any other controls such as a heading control or a roll angle control were performed. Both the desired roll and yaw rates P_c, R_c were set to 0. The nominal ailerons deflection angle $da_{Pullnom}$ and the rudders deflection angle $dr_{Pullnom}$ were controlled to follow the roll and yaw rates P, R to the desired roll and yaw rates P_c, R_c respectively by the following proportional-integral controllers:

$$da_{Pullnom} = Kap_{Pull}(P_c - P) + KaIp_{Pull}\sum(P_c - P)\Delta t \quad (4)$$
$$dr_{Pullnom} = Krr_{Pull}(R_c - R) + KrIr_{Pull}\sum(R_c - R)\Delta t \quad (5)$$

here, Krr_{Pull} and $KrIr_{Pull}$ were the yaw rate proportional and integral gains for the rudder in the roll phase. In the pull-up phase, the elevator deflection angle was still fixed to -15 degrees.

In the glide phase, the control surfaces were controlled to fly toward the desired direction. The desired roll and yaw rates P_c and R_c were obtained as follows:

$$P_c = A_1\psi_{E\,lim} \quad (6)$$
$$R_c = A_2\psi_{E\,lim} \quad (7)$$

here, A_1 and A_2 are gains. $\psi_{E\,lim}$ is a difference between desired and actual headings. Its absolute value was limited within 50 degrees. The nominal ailerons and rudder deflection angles $da_{Glidenom}$ and $dr_{Glidenom}$ were controlled to follow the roll and yaw rates P, R to the desired roll and yaw rates P_c, R_c respectively by the following PI controllers:

$$da_{Glidenom} = Kap_{Glide}(P_C - P) + KaIp_{Glide}\sum(P_C - P)\Delta t \quad (8)$$
$$dr_{Glidenom} = Krr_{Glide}(R_C - R) + KrIr_{Glide}\sum(R_C - R)\Delta t + Kr\psi\psi_{Elim} \quad (9)$$

here, $Kr\psi$ is the heading proportional gain for the rudder. The elevator deflection angle was fixed to -7, -9, and -14 degrees for each glide sub-phase. They correspond to the trim angle of 2, 4, and 6 degrees.

In this flight profile, the dynamic pressure q varies widely from zero to several hundred Pa. The effectiveness of the control surface is depends on the dynamic pressure. Therefore, the correction factor for the dynamic pressure C_q was multiplied to the nominal defection angle of the control surface.

$$C_q = q_s / \max(q, 50) \quad (10)$$

Here, the standard dynamic pressure q_s was set to 120 Pa for the roll and pull-up phases and 58 Pa for the glide phase based on the nominal dynamic pressures in each phase. If the dynamic pressure was less than 50 Pa, the denominator of Eq. (10) was replaced to 50 Pa to avoid divergence. The threshold pressure 50 Pa was determined as a sufficiently low and well observable value using ADS.

The bandpass filter was used to the output of the rate gyro. Its passband was set from 0.001 Hz to 6 Hz based on the prior examination. If the deflection angle reached its mechanical limit, the integral was paused. All gains for PI controller were obtained through a optimization [4,5].

4 Uncertainties

The number of the defined uncertainties was 136. They can be grouped into five: aerodynamic models, initial conditions, gust wind conditions, characteristics of sensors for control, and characteristics of sensors for others. Each uncertainty was basically expressed using a normal random number and defined by given average and standard deviation. However, some uncertainties such as an initial heading were expressed as a uniform random number. Each uncertainty parameters are shown in the appendix. The uncertainties about a deformation were set to relatively large value because the stiffness of the Mars airplane was low to be lightweight to fly in the rare Martian atmosphere.

5 Success Criteria

Two groups of the criteria were defined. One was for a safety and another was for a measurement quality.

Six criteria for a safety were defined as shown in Table 1. The criteria of the moving distance and the heading were defined to keep the airplane away from people. The maximum and minimum lift forces were limited to prevent from destructing the wing. The limitation of the Mach number and sideslip angle were based on the available range of the aerodynamic characteristics data for the simulation.

Table 1. Safety criteria

Parameters	Limits	
Moving distance from release point to land direction	10	km
Absolute difference of airplane heading from desired direction at end of pull-up phase	60	deg
Maximum positive lift	300	N
Minimum negative lift	-300	N
Maximum Mach number	0.7	
Maximum absolute sideslip angle	30	deg

Sixteen criteria for a measurement quality were defined as shown in Table 2. In this high altitude flight test, aerodynamic characteristics at any angle of attack were acceptable as a first trial. In same reason, acceptable range of the average values of the sideslip angle, the Reynolds number, and the Mach number were wide. The criteria for the rotational motion, standard deviation, and the main frequency were defined for the judgement of the quasi-steady condition. The criterion of the standard deviation of the measured lift coefficient was a requirement of this high altitude flight test.

Table 2. Measurement criteria

Parameters	Average	Standard deviation ×3	Main Frequency
Angle of attack	-	1 deg	0 ~ 2 Hz
Sideslip angle	0±10 deg	5 deg	-
Reynolds number	$(5\pm4)\times10^4$	-	-
Mach number	0 ~ 0.7	-	-
Roll rate	0±10 deg/s	20 deg/s	-
Pitch rate	0±10 deg/s	20 deg/s	0 ~ 2 Hz
Yaw rate	0±10 deg/s	20 deg/s	-
Lift coefficient	-	10%	-

6 Flight Simulation

The principal dimensions of the airplane for the flight test are shown in Table 3. The inertial matrix was obtained using the 3D-CAD drawings. The aerodynamic model was established based on the wind tunnel testing result of the scale model [6]. The control period was 0.05 second. Therefore the time step of the simulation was set to 0.005 second. The solver was 4^{th} order Runge-Kutta method. In the nominal condition, the airplane was released from the gondola with aiming its nose downwards. Here, the triaxial velocities and the angular rates were zero.

Table 3. Principal dimensions.

Items	Values	Units
Airplane length	2.00	m
Wing span	2.40	m
Chord length	0.49	m
Height	0.43	m

The sensor outputs that were used for control were calculated from the true values using sensor model. Figure 1 shows a measured value generation process. Here, the generation of the measured pressure value is shown as an example.

A first step was to reproduce the sensor output. The true pressure was known from the simulation. The true pressure was converted to the ideal output voltage using a true relation. Here, because the true relation was unknown, the true relation was estimated as a sum of the nominal relation and the uncertainty parameters. Note that the nominal relation was obtained as a result of the calibration test. Then, sensor errors that were defined in the sensor specification were added to the ideal output voltage and the actual sensor output voltage was obtained.

A next step was to reproduce the input for the avionics. The input port of the avionics has a limitation for an acquirable voltage range. In addition, the voltage has to be converted to digital value and it generates a discretization error. Finally the acquired digital value was converted to the measured pressure value using the nominal relation that was obtained in calibration test.

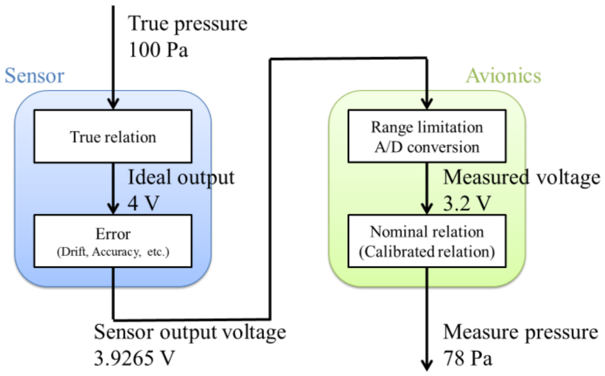

Fig. 1. Measured value generation process.

A one-side confidence interval S for the probability that is obtained by Monte-Carlo simulation can be expressed as follows:

$$S = K_{\alpha/2}\sqrt{\frac{p(1-p)}{n}} \tag{11}$$

where α is a significance level. $K_{\alpha/2}$ is a value that shows one-side probability value of $\alpha/2$ on the standard normal distribution. p and n are the sample probability and the sample size, respectively. The sample size n was set to 500 in this simulation. The significance level α was set to 5%, then the $K_{\alpha/2}$ was 1.96. In this condition, when the sample probability p is 90% as an example, the true value of the probability is within the sample probability p±2.6% with the probability of 95 (= 100 - α) %.

7 Results and Discussion

Figure 2 shows final position and condition of the safety criteria. Almost all result satisfied the safety criteria. The total success probability for a safe flight was 95±2%. Figure 3 shows histograms for each safety criterion parameter with its limit. All case satisfied the safety criteria of the moving distance to land direction and the heading at end of pull-up phase. The safety criteria that shows the worst success rate was the maximum Mach number.

Figure 4 shows histograms for each measurement criterion parameter with its limit. Here, the results of the second glide sub-phase are shown as an example. The total success probability for the measurement quality in the second glide sub-phase was 93±2%. Based on the similar analysis, the total success probability for the measurement quality in the entire glide phase was 77±2%. Also, the measurement success probability that succeeding at least one of the glide sub-phases was 97±2%.

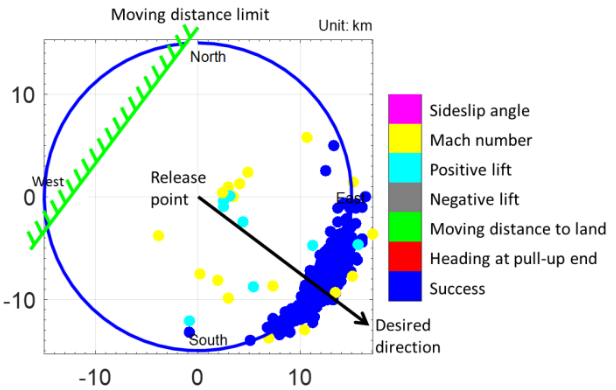

Fig. 2. Final position and safety condition.

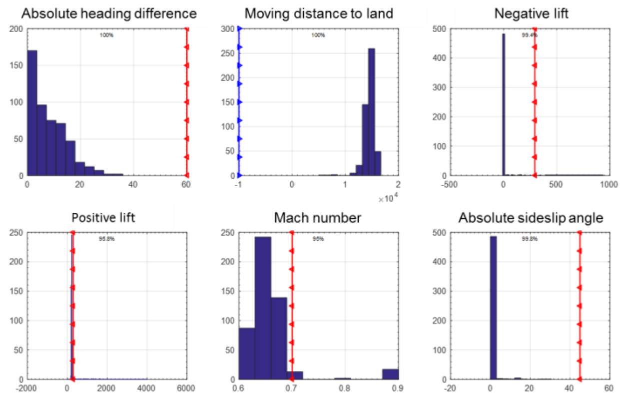

Fig. 3. Histograms for each safety criterion parameter with its limit.

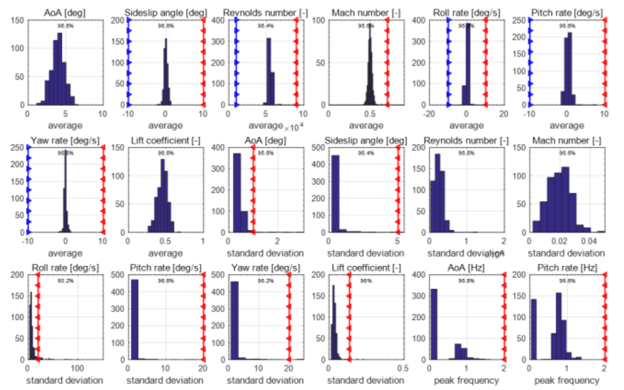

Fig. 4. Histograms for each measurement criterion parameter with its limit at second glide sub-phase.

8 Conclusion

A Monte-Carlo simulation with 136 uncertain parameters was conducted to evaluate the control law of the airplane for the high altitude flight test. The total success probability for safe flight was 95±2%. The effect of the Mach number limitation was the largest. The measurement success probability that succeeding at least one of the glide sub-phases was 97±2%. These results suggests that the control law has sufficient robustness for the flight test.

References

[1] Guynn M D, Croom M A, Smith S C, Parks R W, and Gelhausen P A. Evolution of a Mars Airplane Concept for the ARES Mars Scout Mission. *Proceedings of the 2nd AIAA Unmanned Unlimited Systems, Technologies, and Operations*, San Diego, CA, USA, AIAA paper 2003-6578, 2003.

[2] Nagai H, Oyama A. Development of Japanese Mars Airplane. *Proceedings of the 67th International Astronautical Congress*. Guadalajara, Mexico, IAC-16-A3.3A.5x35104, Sep. 2016.

[3] Oyama A, et al. Flight System of Mars Airplane Balloon Experiment-1 (MABE-1). *Proceedings of the 31st International Symposium on Space Technology and Science*, Matsuyama, Ehime, Japan, 2017-k-42, June. 3-9, 2017.

[4] Fujita K, Tokutake H, Nagai H, Oyama A. Flight Control Parameter Design for Mars Airplane Balloon Experiment-1 (MABE-1) Using Evolutionary Computation. *Proceedings of the 31st International Symposium on Space Technology and Science*, Matsuyama, Japan, 2017-k-44, June. 3-9, 2017.

[5] Fujita K, Oyama A, Tokutake H, Nagai H. Evolutionary Computation Approach for Automatic Gain Tuning of Mars Airplane Balloon Experiment-1 (MABE-1). *Proceedings of the 14th International Conference on Flow Dynamics*, Sendai, Japan, Nov. 1-3, 2017.

[6] Anyoji M, et al. Planetary Atmosphere Wind Tunnel Tests on Aerodynamic Characteristics of a Mars Airplane Scale Model. *Transactions of the Japan Society for Aeronautical and Space Sciences*, Aerospace Technology Japan, Vol. 12, No. ists29 pp. Pk_7-Pk_12, 2014. doi: 10.2322/testj.12.Pk 7.

8 Contact Author Email Address

mailto:fujita.koji@tohoku.ac.jp

Copyright Statement

Appendix

Definitions of the uncertainties

Number	Name	3 σ equivalent value	Unit
1	C_M measurement error in wind tunnel test at Re = 3.3 × 10^4	0.0245	-
2	C_M measurement error in wind tunnel test at Re = 7.0 × 10^4	0.006	-
3	C_Y measurement error in wind tunnel test	30	%
4	C_l measurement error in wind tunnel test	30	%
5	C_n measurement error in wind tunnel test	30	%
6	Angle of attack error in wind tunnel test for longitudinal force	1	deg
7	Angle of attack error in wind tunnel test for lateral force	1	deg
8	Manufacturing error of aileron deflection angle	2	deg
9	Manufacturing error of elevator deflection angle	2	deg
10	Manufacturing error of rudder deflection angle	2	deg
11	Dihedral deformation at load factor of 1	1	deg
12	Difference of aerodynamic twist deformation	1	deg
13	Manufacturing error of vertical tail angle	0.3	deg
14	C_{lp} estimation error	0-200	%
15	C_{lr} estimation error	0-200	%
16	C_{Mq} estimation error	0-200	%
17	Moment of inertia error (X-axis)	20	%
18	Moment of inertia error (Y-axis)	20	%
19	Moment of inertia error (Z-axis)	20	%
20	Products of inertia error (XZ axis)	20	%
21	Aerodynamic deformation of elevator	4	%
22	Aerodynamic deformation of rudder	4	%
23	Aerodynamic deformation of aileron	8	%
24	Mass error	5	%
25	C.G. position error (X-axis)	0.003	m
26	C.G. position error (Y-axis)	0.003	m
27	C.G. position error (Z-axis)	0.01	m
28	Main wing incident angle error	0.5	deg
29	Tail boom bending ratio per force	0.1	deg/N
30	Wing tip angle difference (No wind)	0.42	deg
31	Dihedral error (No wind)	0.17	deg
32	Horizontal tail incident angle error	0.42	deg
33	Initial roll rate	30	deg/s
34	Maximum amplitude of oscillation of gondola	20	deg
35	Gondola oscillating direction	360	deg
36	Gondola direction	360	deg
37	Initial pitch angle	20	deg
38	Initial yaw angle	360	deg
39	Pressure change due to weather	133.5	Pa
40	Temperature change due to weather	10	degC
41	Density change due to weather	0.0017	kg/m^3
42	Gust wind intensity (X-axis)	4	m/s
43	Gust wind intensity (Y-axis)	4	m/s
44	Gust wind intensity (Z-axis)	4	m/s
45	Airplane magnetometer accuracy	10	deg
46	Sensitivity error of roll rate gyro	0.0004	V/(deg/s)
47	Sensitivity error of pitch rate gyro	0.0004	V/(deg/s)
48	Sensitivity error of yaw rate gyro	0.0004	V/(deg/s)
49	Offset of roll rate gyro	0.02	V
50	Offset of pitch rate gyro	0.02	V
51	Offset of yaw rate gyro	0.02	V
52	Nonlinearity error of roll rate gyro	0.6	deg/s
53	Nonlinearity error of pitch rate gyro	0.6	deg/s
54	Nonlinearity error of yaw rate gyro	0.6	deg/s
55	Error rate of roll rate gyro due to acceleration	0.0204	(deg/s)/(m/s^2)

56	Error rate of pitch rate gyro due to acceleration	0.0204	(deg/s) /(m/s^2)
57	Error rate of yaw rate gyro due to acceleration	0.0204	(deg/s) /(m/s^2)
58	Angle of attack calibration error of Air Data Sensor	5	%
59	Dynamic pressure calibration error (1) of Air Data Sensor	5	%
60	Dynamic pressure calibration error (2) of Air Data Sensor	5	%
61	Roll rate gyro error due to supply voltage	1	deg/s/V
62	Pitch rate gyro error due to supply voltage	1	deg/s/V
63	Yaw rate gyro error due to supply voltage	1	deg/s/V
64	Temperature change of dynamic pressure sensor	10	degC
65	Error of register (1) for dynamic pressure sensor	5	%
66	Error of register (2) for dynamic pressure sensor	5	%
67	Measurement error of temperature of dynamic pressure sensor	2.5	degC
68	Sensitivity error of dynamic pressure senor	5	%
69	Offset error of dynamic pressure sensor	0.195	Pa
70	Temperature sensitivity of dynamic pressure	0.0006	V/degC
71	Span error of dynamic pressure sensor	0.0003	1/degC
72	Temperature drift rate of roll rate gyro	0.0885	(deg/s) /degC
73	Temperature drift rate of pitch rate gyro	0.0885	(deg/s) /degC
74	Temperature drift rate of yaw rate gyro	0.0885	(deg/s) /degC
75	Gondola magnetometer accuracy	10	deg
76	Terrestrial magnetism declination error	0.5	deg
77	Terrestrial magnetism inclination error	0.5	deg
78	Supply voltage error for *X*-accelerometer	0.2	%
79	Supply voltage error for *Y*-accelerometer	0.2	%
80	Supply voltage error for *Z*-accelerometer	0.2	%
81	Avionics temperature change	10	degC
82	*X*-accelerometer error due to supply voltage	4	%/V
83	*Y*-accelerometer error	4	%/V

	due to supply voltage		
84	*Z*-accelerometer error due to supply voltage	4	%/V
85	Temperature drift rate of *X*-accelerometer	0.0196	(m/s^2) /degC
86	Temperature drift rate of *Y*-accelerometer	0.0196	(m/s^2) /degC
87	Temperature drift rate of *Z*-accelerometer	0.0196	(m/s^2) /degC
88	Temperature change rate of *X*-accelerometer sensitivity	0.0077	%/degC
89	Temperature change rate of *Y*-accelerometer sensitivity	0.0077	%/degC
90	Temperature change rate of *Z*-accelerometer sensitivity	0.0077	%/degC
91	Sensitivity error of *X*-accelerometer calibration	5	%
92	Sensitivity error of *Y*-accelerometer calibration	5	%
93	Sensitivity error of *Z*-accelerometer calibration	5	%
94	Offset error of *X*-accelerometer calibration	5	%
95	Offset error of *Y*-accelerometer calibration	5	%
96	Offset error of *Z*-accelerometer calibration	5	%
97	Sideslip angle calibration error of Air Data Sensor	5	%
98	Voltage offset error of calibration of measured angle of attack	0.11	deg
99	Voltage sensitivity error of calibration of measured sideslip angle	5	%
100	Voltage offset error of calibration of measured sideslip angle	0.14	deg
101	Initial temperature change of differential pressure sensor for angle of attack and sideslip	10	degC
102	Initial temperature change of static pressure sensor	10	degC
103	Temperature sensitivity of differential pressure for angle of attack	0.006	V/degC
104	Temperature sensitivity of differential pressure for sideslip angle	0.006	V/degC
105	Span error of differential pressure sensor for angle of attack due to temperature change	0.002	1/degC
106	Span error of differential	0.002	1/degC

	pressure sensor for sideslip angle due to temperature change		
107	Angle of attack calibration error of conversion from differential pressure to voltage	0.0086	V
108	Sideslip angle calibration error of conversion from differential pressure to voltage	0.0062	V
109	Resistor error for differential pressure sensor for angle of attack (1)	1	%
110	Resistor error for differential pressure sensor for sideslip angle (1)	1	%
111	Resistor error for differential pressure sensor for angle of attack (2)	1	%
112	Resistor error for differential pressure sensor for sideslip angle (2)	1	%
113	Temperature measurement error of pressure sensor for angle of attack	2.5	degC
114	Temperature measurement error of pressure sensor for sideslip angle	2.5	degC
115	Sensitivity error of static pressure sensor	5	%
116	Offset error of static pressure sensor	158	Pa
117	Accuracy of static pressure sensor	0.003	V
118	Temperature sensitivity of static pressure sensor	0.001	V/degC
119	Calibration error of total temperature sensor	3	degC
120	Temperature error rate of total temperature sensor	0.05	degC /degC
121	Gain error of total temperature sensor	1.5	%
122	Sensitivity error of potentiometer for left aileron	5	%
123	Offset error of potentiometer for left aileron	2	deg
124	Sensitivity error of potentiometer for right aileron	5	%
125	Offset error of potentiometer for right aileron	2	deg
126	Sensitivity error of potentiometer for elevator	5	%
127	Offset error of potentiometer for elevator	2	deg
128	Sensitivity error of potentiometer for left rudder	5	%
129	Offset error of potentiometer for left rudder	2	deg
130	Sensitivity error of potentiometer for right rudder	5	%
131	Offset error of potentiometer for right rudder	2	deg
132	Inertial sensor position error (*X*-axis)	0.01	m
133	Inertial sensor position error (*Y*-axis)	0.01	m
134	Inertial sensor position error (*Z*-axis)	0.01	m
135	Alignment error of pitot tube (angle of attack)	0.02	deg
136	Alignment error of pitot tube (sideslip angle)	0.03	deg